Environmental Science and Pollution Research (2023) 30:53807–53816
https://doi.org/10.1007/s11356-023-26222-y

RESEARCH ARTICLE

Modifications to microplastics by potassium ferrate(VI): impacts on sorption and sinking capability in water treatment

Ruijuan Liu[1,2] · Yuheng Chen[2] · Xinni Wu[1,2] · Jianwei Fu[2] · Huase Ou[1,2]

Received: 28 June 2022 / Accepted: 26 February 2023 / Published online: 3 March 2023

Abstract

Pre-treatment (oxidation) may induce potential modifications to microplastics (MPs), further affecting their behaviors and removal efficiency in drinking water treatment plants. Herein, potassium ferrate(VI) oxidation was tested as a pre-treatment for MPs with four polymer types and three sizes each. Surface oxidation occurred with morphology destruction and oxidized bond generation, which were prosperous under low acid conditions (pH 3). As pH increased, the generation and attachment of nascent state ferric oxides (Fe_xO_x) gradually became dominant, making MP-Fe_xO_x complexes. These Fe_xO_x were identified as Fe(III) compounds, including Fe_2O_3 and FeOOH, firmly attaching to the MP surface. Using ciprofloxacin as the targeted organic contaminant, the presence of Fe_xO_x enhanced MP sorption dramatically, e.g., the kinetic constant K_f of ciprofloxacin raised from 0.206 (6.5 μm polystyrene) to 1.062 L g^{-1} (polystyrene-Fe_xO_x) after oxidation at pH 6. The sinking performance of MPs was enhanced, especially for small MPs (< 10 μm), which could be attributed to the increasing density and hydrophilicity. For instance, the sinking ratio of 6.5 μm polystyrene increased by 70% after pH 6 oxidation. In general, ferrate pre-oxidation possesses multiple enhanced removals of MPs and organic contaminants through adsorption and sinking, reducing the potential risk of MPs.

Keywords Plastic debris · Advanced oxidation processes · Nanoplastics · K_2FeO_4 · Pollution control

Introduction

Microplastics (MPs) have spread throughout the world for a long time, but only now has their presence come to the public perception. They are defined as plastic debris smaller than 5 mm with different shapes, such as grain, sheet, and filiform (Law and Thompson 2014). MPs have garnered particular attention due to their persistence, mobility, and, most importantly, "cocktail" feature (Guzzetti et al. 2018). That is, they can adsorb various microorganisms, heavy metals, and organic matter, forming contaminant complexes, aggravating the uncertainty of environmental risk (Vethaak and Legler 2021). As an important part of natural environmental systems, the freshwater ecosystem also suffers from MP pollution. Recent evidence indicated the existence of MPs in worldwide lakes (Anderson et al. 2017; Zbyszewski and Corcoran 2011), rivers (Koelmans et al. 2019), ground waters (Mintenig et al. 2019), estuaries (Lima et al. 2014) and sediments (Lima et al. 2014). For example, the concentration of MPs in rivers ranged from 0.021×10^6 to 7.2×10^6 particles m^{-3} (Di and Wang 2018; Lahens et al. 2018; Liao et al. 2020; Zhang et al. 2017), while the one in lakes ranging from 0.01×10^6–6.8×10^6 particles km^{-2} (Su et al. 2016; Uurasjarvi et al. 2020). Furthermore, up to 10^2 particles kg^{-1} MPs were detected in sediment samples (Ta and Babel 2020; Vianello et al. 2013). MP pollution in freshwaters may pose ecological risks and threats to drinking water safety for modern society.

Along with the source water, MPs are transferred to urban engineered water systems, with the first step at drinking water treatment plants (DWTPs). To improve the removal of MPs and evaluate the potential threats of MPs to drinking water safety, the modifications on characteristics of MPs induced by various treatment processes require further

Responsible Editor: Ricardo A. Torres-Palma

✉ Huase Ou
touhuase@jnu.edu.cn

[1] Guangdong Key Laboratory of Environmental Pollution and Health, School of Environment, Jinan University, Guangzhou 511443, China

[2] Center for Environmental Microplastics Studies, Jinan University, Guangzhou 511443, China

investigation. Pre-treatments are applied at the beginning of DWTPs. The most common technics are pre-oxidation, e.g., chlorination, ozonation, and potassium permanganate ($KMnO_4$) oxidation (Xie et al. 2016), which have been suggested as the assistant methods for DWTPs (2006 2011). These methods become the first stage to face MP pollutants, and most contain deconstructive chemical reactions, which could change the characteristics of MPs. Lin et al. (2022) reported that polystyrene (PS) tends to float on the water after chlorination, demonstrating a decreased sinking ratio. In our previous study, $KMnO_4$ oxidation was proved to add nano-MnO_2 onto MPs, improving the sedimentation of PS, polyethylene terephthalate (PET), and polyvinyl chloride (PVC), but not polyethylene (PE) (Chen et al. 2022). Compared to the pristine MPs, the sinking ratio of treated MPs (6.5 μm) increased by 30% (PET), 20% (PVC), and 30% (PS). Furthermore, the sorption of organic contaminants by MPs was also changed by heat-activated $K_2S_2O_8$ (Liu et al. 2019) and radical-based UV (Lin et al. 2020). Thus, pre-oxidation could induce evident aging and destruction of MPs, affecting their behavior and removal efficiency in subsequent treatment processes.

In recent years, ferrate ($Fe^{VI}O_2^{2-}$, Fe(VI)) oxidation, usually with potassium ferrate (K_2FeO_4), has received increasing attention due to its easily accessible and environmentally friendly nature in water treatment application (Sharma et al. 2015). Ferrate was explored for multipurpose actions, i.e., degradation of organic contaminants (Zhou and Jiang 2015) and inactivation of algae/cyanobacteria (Fan et al. 2018; Ma and Liu 2002). This relied on the highly oxidative activity of Fe(VI) with a redox potential of 2.20 V, which was higher than hypochlorite (1.48 V), ozone (2.08 V), and permanganate (1.68 V) under acidic conditions. Furthermore, the portfolios of ferrates also included coagulants, which relied on the flocs consisting of nascent Fe(III) oxides/hydroxides (Lv et al. 2018), enhancing the removal efficiency of particles in the next coagulation-sedimentation stage (Jun and Wei 2002). Most importantly, ferrate produces no mutagenic by-products (Xie et al. 2016), and even reduces the generation potential of chlorinated disinfection by-products (Jiang et al. 2016). These multipurpose actions endow ferrates with unique advantages in removing organic contaminants and particles from water. However, ferrate-induced modifications on MPs have not yet been realized. Ferrate pre-oxidation may induce multiple unknown interactions with MPs, resulting in unexpected behaviors of MPs in ensuing water treatment processes.

Herein, this study aims to evaluate the modifications to MPs by ferrate(VI) and explore the impacts on sorption and sinking in DWTPs. Investigating its intrinsic mechanisms would be significant for predicting the migration and transport patterns of MPs in the aquatic ecosystems. The lab-scale potassium ferrate oxidation was conducted, while four polymers, including PE, PET, PS, and PVC, were selected as targeted MPs. The surface morphology, chemical, and hydrophobic variations were investigated to determine the MP destruction induced by ferrate oxidation. Furthermore, ciprofloxacin (CIP) was selected as the targeted organic contaminant for the sorption performance since it has been detected in water supplies and found to be environmentally harmful (Hettithanthri et al. 2022). To further understand the behavior of MPs after pre-treatment, the modification of sinking patterns was evaluated.

Experimental

Materials

Four polymers, PE, PET, PS, and PVC, were acquired from Goodfellow Cambridge Ltd. Small MPs (< 1 mm) were detected in DWTPs (Novotna et al. 2019). Thus, MP particles with 6.5, 100, and 500 μm were prepared. Analytical-grade K_2FeO_4, methanol, and ethanol were obtained from Sinopharm. Ultrapure water was acquired from Fisher (USA). A source water from a DWTP was obtained as the background water matrix (Table S1).

Aging of MPs

To simulate the actual MPs in the natural environment, MPs used for experiments in the current study were all treated by artificial aging. Pristine MPs were sealed in a box with a customized glass cover that could be penetrated by ultraviolet light. The MP-containing box was placed outdoors under natural sunlight irradiation for 60 days.

Ferrate oxidation

Oxidation experiments were conducted in 250-mL glass beakers using vortex mixers (60 rpm, 25.0 ± 0.2 °C), and in phosphate buffer which exhibited little effect on the oxidation ability of Fe(VI) species (Huang et al. 2018). Before reactions, approximately 100 mL of buffered reaction solution was added to each beaker, and then, a number of MPs were added. The MP concentration applied was 1 mg L^{-1}, which contains ~ 2.5×10^2–~ 5.5×10^2 particles L^{-1} (6.5 μm). This is close to that detected in DWTP source waters (~ 10^2 particles L^{-1}) (Novotna et al. 2019). A stock solution of Fe(VI) (typically 100 μM) was prepared immediately by solving K_2FeO_4 into 5 mM Na_2HPO_4 and 1 mM borate buffer (pH = ~ 9.1) (Yang et al. 2018). The ferrate oxidation was started by adding a given amount of the stock Fe(VI) solution (pH = ~ 9.1) into the reaction system with rapid mixing. Stock Fe(VI) solution was used within 10 min after being prepared. The initial Fe(VI) concentration was set to 10 mg L^{-1} (Zhou et al. 2014). After adding the

stock Fe(VI) solution and the MPs, the pH of the solution was adjusted as needed. According to the Fe(VI) species distribution and pH function (Sharma et al. 2015), reaction solutions with pH at 3, 6, 8, and 11 were prepared using H_2PO_4, NaOH, and phosphate buffer. Sampling was conducted at a specific time, followed by filtration with 0.45-μm hydrophilic filters. The obtained MPs were washed with ultrapure water. Finally, the MP samples were separated from filters and dried under 40 °C overnight. All the experiments were performed in triplicate.

Analytical methods for MPs

Morphologies were detected by a scanning electron microscope (SEM). The chemical composition of MP surfaces was analyzed by X-ray photoelectron spectrometer (XPS), and micro-Fourier transform infrared spectrometer (FTIR) was employed to analyze (Text S1). MP density was determined using a PoreMaster33GT mercury porosimeter. To determine the mass of MPs, a method developed in our previous study was applied (Chen et al. 2022).

Two-dimensional correlation analysis

A two-dimensional correlation analysis (2D-COS) was applied for FTIR. The FTIR spectra were recorded in a range of 4000–400 cm^{-1}. Since no apparent response variation was detected in the range of 3000–2000 cm^{-1}, 2D COS was carried out using the FTIR spectra in the range of 2000–600 cm^{-1} over time. The analysis of 2D-COS followed a method developed by Lasch et al. using 2D Shige software (Lasch and Noda 2019). After calculation, 2D-COS synchronous and asynchronous maps were obtained to decode the evolution of organic functional groups on MP surfaces.

XPS analysis

XPS calculation involved charge correction, smoothing, non-linear Shirley-type background subtraction, and curve fitting. The C1s binding energies at 284.6 eV were used as the standard. A deconvolution was processed for XPS peaks using XPS PEAK with Lorentzian-Gaussian functions after subtraction of a Shirley background (Yamashita and Hayes 2006). Relative intensities (areas) of the sub-peaks were determined using Gaussian–Lorentzian functions embedded in XPS PEAK. As a result, the evolution of different components from an element can be investigated. The relative area ratios (AR) between different forms of Fe (such as Fe_2O_3 and FeOOH) are calculated by:

$$\mathrm{AR} = \mathrm{area}_1/\mathrm{area}_2 \quad (1)$$

where area_1 and area_2 are the peak areas of Fe_2O_3 and FeOOH, respectively.

Sorption experiment

Ciprofloxacin ($C_{17}H_{18}FN_3O_3$, MW = 331.4 g mol^{-1}) was used for the sorption test. The sorption experiment was conducted using a procedure developed in our published study (Lin et al. 2020). The treated MPs were obtained in "Ferrate oxidation" section.

Sinking experiment

The sinking performance was evaluated based on a previously developed method (Lin et al. 2022). Specifically, MPs were treated by ferrate oxidation using the DWTP source water as background matrixes. Subsequently, MPs were separated by syringe-filter kits, washed, and dried at 40 °C. Approximately 100 mg of MPs was soaked in the source water without any chemical addition and stirred (30 min). And then, a 2-h stand was conducted. We separated the floating MPs (M_{floating}, on the surface and suspending in the water) and the sinking MPs (M_{sinking}, on the bottom). A customized method was applied to quantify the mass of these two-part MPs (Chen et al. 2022). The sinking ratio of MPs can be obtained:

$$\text{Sinking ratio} = \frac{M_{\mathrm{sinking}}}{M_{\mathrm{sinking}} + M_{\mathrm{floating}}} \quad (2)$$

Results and discussion

Morphology

All aged MPs presented smooth surfaces with complete and clear boundaries but no cracks and bumps (Fig. 1). After the ferrate oxidation, some surface morphological variations were observed. In the low-magnification SEM images, only a few differences in size and integrity were found. Notably, many nano-scale crystals were attached on all four MP surfaces, forming rough and uneven surfaces. Previous studies reported nano-scale crystal structure after ferrate oxidation (Prucek et al. 2013; Yang et al. 2018). By amplification, these surface crystals presented irregular shapes. As energy-dispersive spectrum (Fig. S1) showed, these attachments mainly contained iron and oxygen, indicating that they could be the nascent state ferric oxides (Fe_xO_x) adhering to the MP surface during the ferrate oxidation. Similar ferric oxides were reported in other studies (Kralchevska et al. 2016; Yang et al. 2018; Zheng et al. 2021). Of note, though the MP samples had been washed with ultrapure water after ferrate oxidation, these ferric oxides still existed, indicating their firm attachment on the MP surfaces. Thus, the MPs were transformed into MP-Fe_xO_x complexes. In addition, the smooth surfaces disappeared with obvious alternations, including cracks

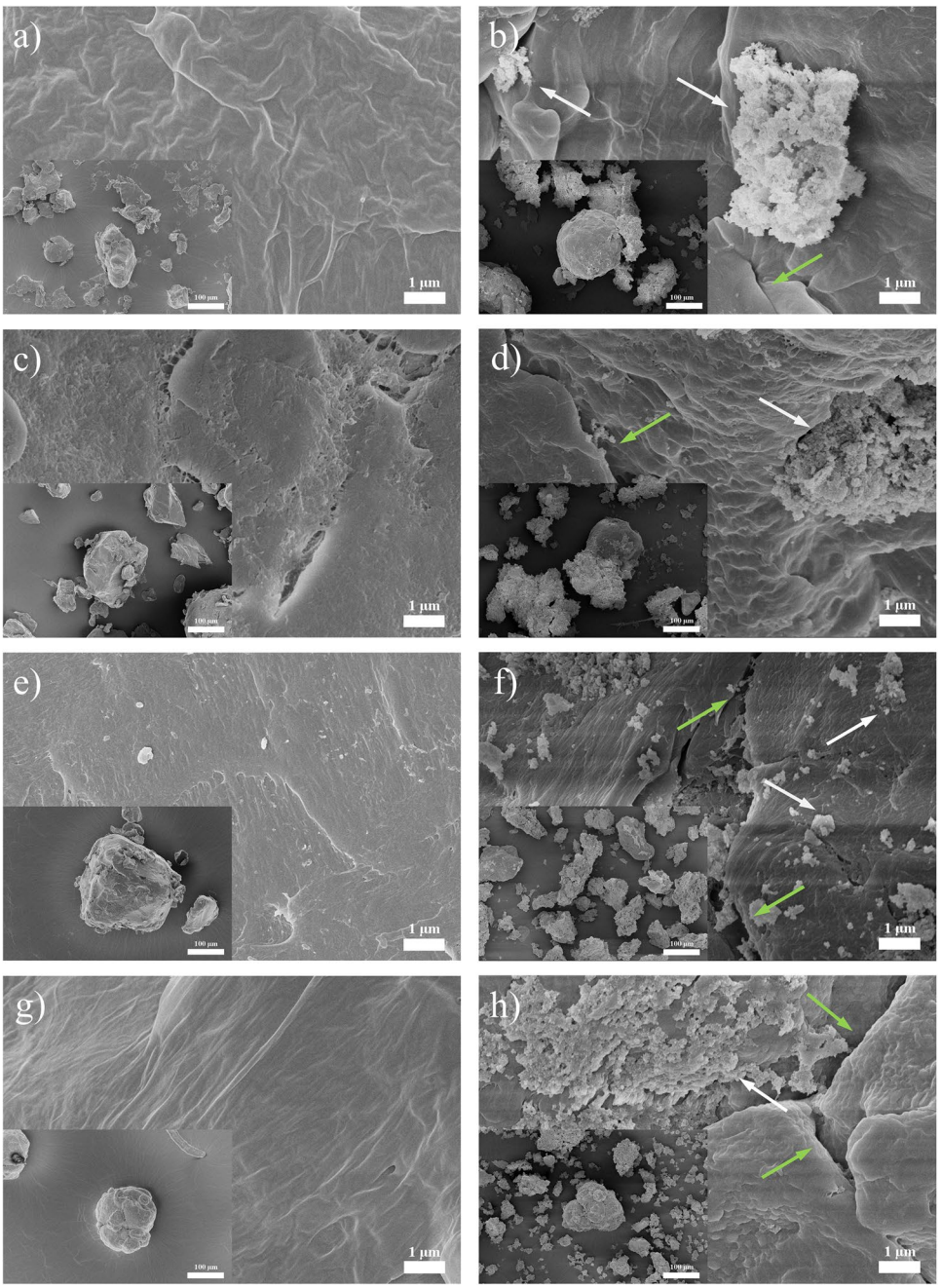

Fig. 1 Microscopical image of microplastics after ferrate oxidation. Experimental conditions: $[K_2FeO_4]_0 = 10$ mg L^{-1}, pH = 6, reaction time = 30 min, MP size = 200 µm. **a**, **b** Aged and oxidized polyethylene; **c**, **d** aged and oxidized polyethylene terephthalate; **e**, **f** aged and oxidized polystyrene, and **g**, **h** aged and oxidized polyvinyl chloride. White arrow indicates nascent state ferric oxides, and green arrow indicates destruction on surface

(Fig. 1d and f), wrinkles (Fig. 1h), and protuberances (Fig. 1b). It could be ascribed to surface destruction by ferrate oxidation.

Surface chemical variations

The ferrate oxidation facilitated a series of oxidized functional groups on the MP surfaces (Figs. 2 and S2). Generally, a prominent broad peak was observed in the range of 3000–3500 cm^{-1} for all MPs after ferrate oxidation. This is the characteristic peak of O–H stretch. FTIR data in time gradient were also obtained (Fig. 2). The broad peak (3000–3500 cm^{-1}) intensity gradually increased with time, suggesting continuous oxidation. Some other characteristic peaks were observed, e.g., ~ 1000 cm^{-1} and 1400 cm^{-1} for PE, 1560–1640 cm^{-1} for PS, indicating C–O, O–H, and other oxidized functional groups.

Two-dimensional COS images (Fig. 3) were applied to further investigate the changes in FTIR characteristic peaks. For PE, two major autopeaks at ~ 1000 cm^{-1} and ~ 1400 cm^{-1}

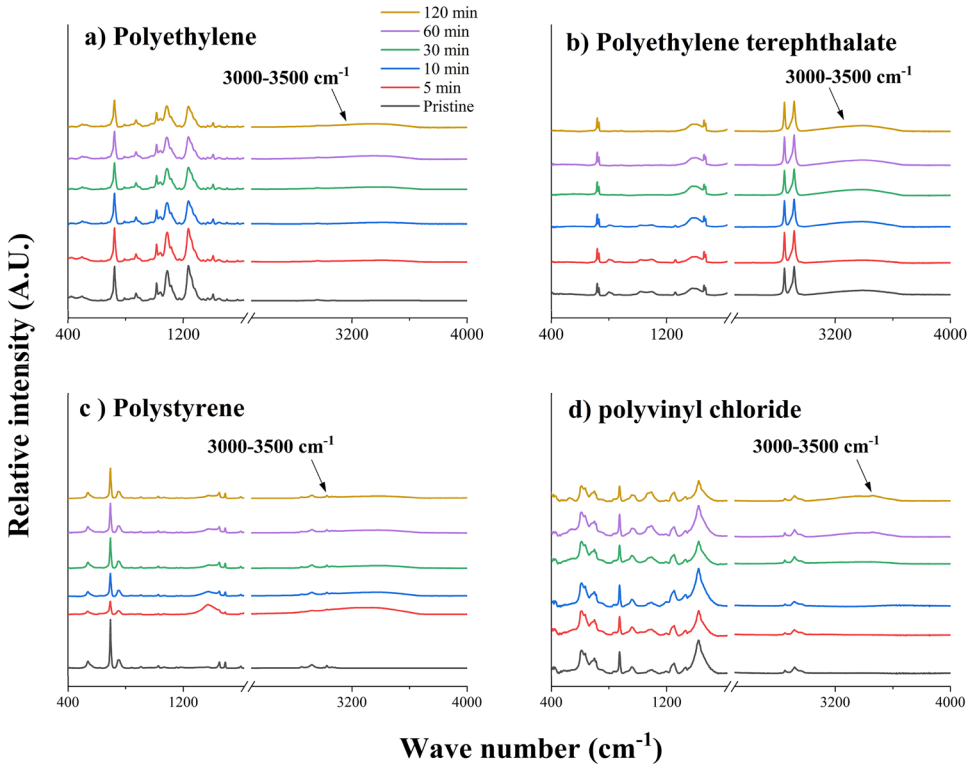

Fig. 2 Fourier transform infrared spectroscopy variations of microplastics. Experimental conditions: $[K_2FeO_4]_0 = 10$ mg L^{-1}, pH = 6, reaction time = 30 min, MP size = 200 μm

were observed in the synchronous map (Fig. 3a), indicating the existence of C–O and –COOH. Based on Noda's rules (Jin et al. 2018), asynchronous correlation spectroscopy indicates the evaluation order of chemical bonds (Mao et al. 2020). In the asynchronous correlation spectrum, the characteristic peak at Ψ (1000, 1400) was positive (Fig. 3b), implying that the generation of C–O was earlier than –COOH.

In the synchronous map of PET (Fig. 3c and d), three major autopeaks at 1070 cm^{-1} (C–O stretching of primary alcohol), 1100 cm^{-1} (C–O stretching of secondary alcohol), and 1275 cm^{-1} (C–O stretching of alkyl aryl ether) were identified. All these peaks suggested that the PET surface was modified after ferrate oxidation. Based on the asynchronous correlation spectrum, the generation sequence was suggested to be 1070, 1100, and 1275 cm^{-1}, indicating that the oxidized PET surface contained various unordered structures.

For PS and PVC, only major autopeaks at 1375 cm^{-1} and 1400 cm^{-1} were observed, respectively. Both of them were associated with C–OH functional groups. The FTIR data and 2D COS analysis generally indicated continuous surface destructions on MPs.

Chemical characteristics of MP-Fe_xO_x complexes

XPS (Fe spectrum) was obtained to confirm the chemical characteristics of the adhesive Fe_xO_x (Figs. 4, S3 and S4). The evolution of four MPs presented similar patterns. Taking PET as an analyzed target, the aged MPs presented no Fe signal. Yet, apparent Fe2p signals were observed after ferrate oxidation (Fig. 4a). Generally, the dominant $Fe2p_{3/2}$ peak had binding energy in the range of 710.8–711.9 eV, suggesting the existence of iron oxides. To determine the valence state of iron oxides, the shape and binding energy of $Fe2p_{3/2}$ satellite peak were investigated. Yamashita et al. (2008) found that the $Fe2p_{3/2}$ satellite peak of Fe(II) presented a shoulder peak, while the one of Fe(III) was usually an independent peak in the range of 715–25 eV. In Fig. 4b, an independent satellite peak was observed for the MP-Fe_xO_x complexes. Thus, the dominant iron oxides on MPs were Fe(III) compounds.

After pH 3 oxidation, the binding energy of $Fe2p_{3/2}$ was ~ 711.9 eV (Fig. 4), which was associated with FeOOH (Fe(III), 710.9–711.9 eV). As the pH increased, the chemical shift of Fe2p gradually appeared. The binding energy of $Fe2p_{3/2}$ shifted to ~ 710.8 eV after pH 11 ferrate oxidation, implying the existence of other forms of iron oxides, such as Fe_2O_3 (710.4–711.6 eV). To further determine the evolution of these two iron oxides, the characteristic peaks of Fe2p were deconvoluted by XPS peak analysis (Fig. 4b), and their peak area ratio (AR, Fe_2O_3 vs. FeOOH) was calculated (Table S2) (Biesinger et al. 2011). The AR value had a positive correlation with the pH value. For example, the AR of PE increased from 1.39 to 1.85 when pH rose from 3 to 11, suggesting that more Fe_2O_3 was generated under alkaline conditions than that

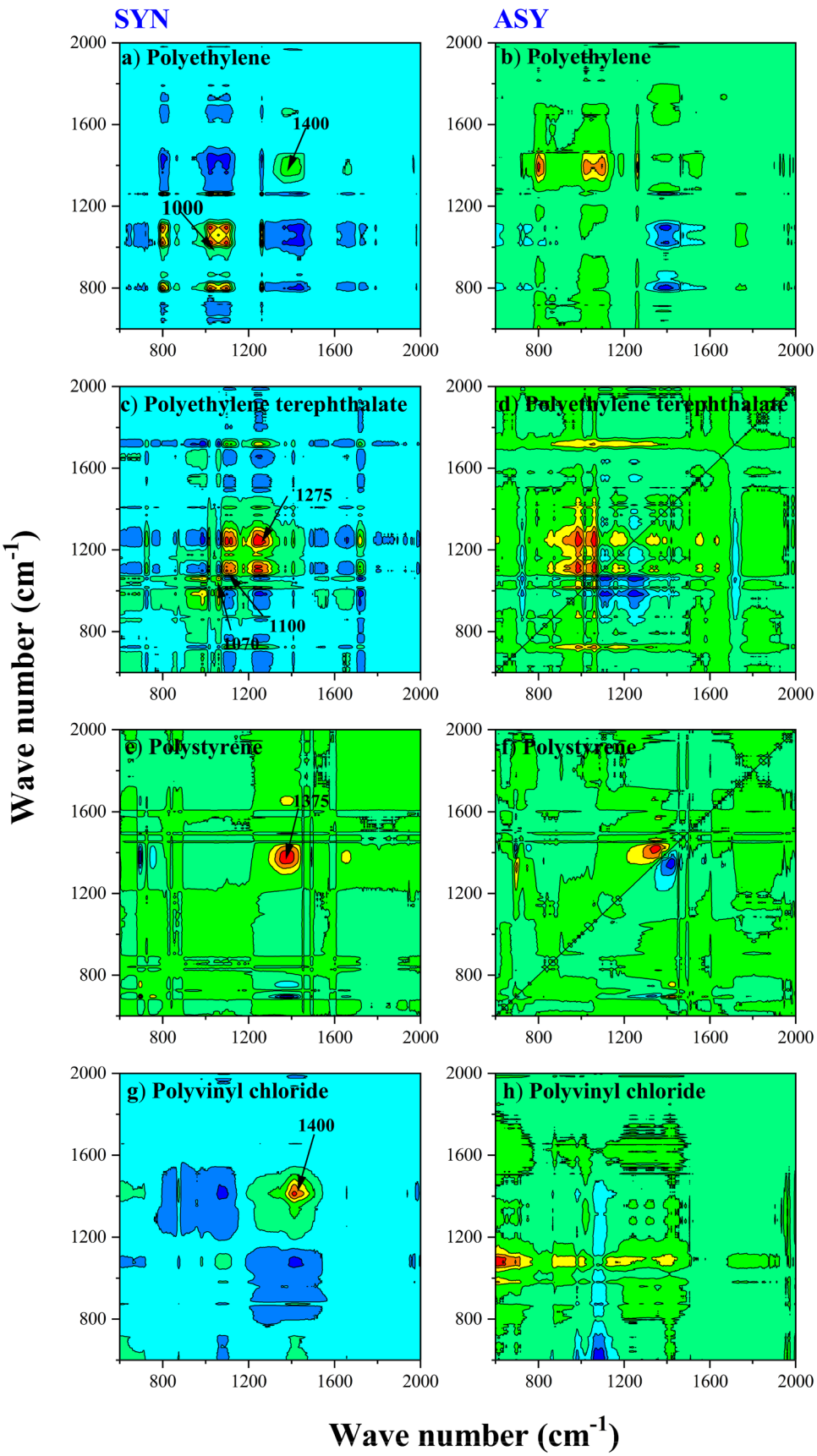

Fig. 3 Two-dimensional COS images. SYN indicates the synchronous map, and ASY indicates the asynchronous map. Experimental conditions: $[K_2FeO_4]_0 = 10$ mg L^{-1}, pH = 6, reaction time = 30 min, MP size = 200 μm

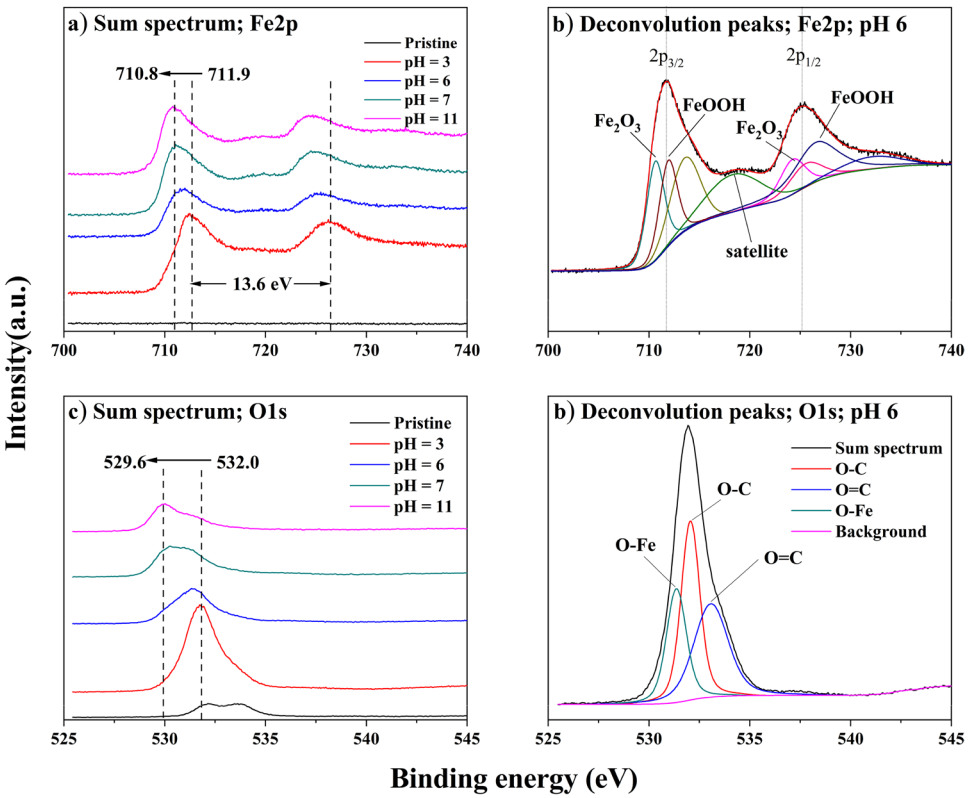

Fig. 4 X-ray photoelectron spectroscopy variations of polyethylene terephthalate. Experimental conditions: $[K_2FeO_4]_0 = 10$ mg L^{-1}, pH = 3, 6, 8, 11, reaction time = 30 min, MP size = 200 μm

under acid conditions. This also implied that the content of Fe_2O_3 in the reaction system gradually increased. In general, the Fe2p spectrum proved that FeOOH and Fe_2O_3 dominated the attached Fe_xO_x on the MP surfaces during ferrate oxidation.

The O1s spectra of aged PET presented slight signals, which may be due to oxidation during artificial aging. Their intensities increased after ferrate oxidation (Fig. 4c). Characteristic O1s peaks at 532.0 eV were observed under pH 3, indicating the existence of carbon–oxygen bonds, i.e., C–O and C = O (Moulder et al. 1992). A chemical shift (1–2 eV) to lower binding energy was observed as pH increased. All MPs presented similar tendencies, indicating that the O–Fe bonds with low-energy O1s spectrum gradually became dominant. This may be due to the chemical characteristic of ferrate oxidation under different pH values. Ferrate is highly oxidative under acidic conditions, resulting in more generation of oxygen containing groups on MPs. It tended to be weak as the pH increased. On the contrary, the generation of Fe_xO_x was enhanced as pH raised. Thus, the peak at 532 eV (O–C bond) shifted to the peak at 530 eV (O–Fe bond).

XPS can only detect the chemical variations on nanometer-level surfaces, while FTIR can go deep into several hundred micrometers. This is why their results were different. The surface of MP-Fe_xO_x complexes was dominated by nano-Fe_xO_x crystals, which XPS determined. Under these crystals, the entire surface of MPs was oxidized. Thus, FTIR reported the existence of C–O and C = O bonds. The transformation from MPs to MP-Fe_xO_x complexes could be accompanied by changes in sorption capacity and sinking performance.

Sorption of organic matter

Sorption of CIP by aged MPs followed the Freundlich model ($R^2 > 0.95$, Fig. 5). Aged MPs only presented weak sorption capacities to CIP, with a K_f at 0.226 L g^{-1} (PET). After ferrate oxidation, the sorption of CIP by these MP-Fe_xO_x complexes was dramatically enhanced (Fig. 5, Table S3). The K_f of PE increased from 0.142 to 0.360 L g^{-1} after pH 6 ferrate oxidation, while K_f of PS rose from 0.206 to 1.062 L g^{-1}. These significant improvements may be attributed to the attachment of Fe_xO_x nanoparticles on MP surfaces. These ferric oxides, including Fe_2O_3 and FeOOH, presented nano-scale and dispersed characteristics with abundant hydroxylated groups on the MP-Fe_xO_x surfaces, endowing them the complicated interactions with organic matter and other contaminants in water through hydrogen bonds and other chemical bonds. Yang et al. (2018) used ferrate to degrade *p*-arsanilic acid, and they found that the released As(V) can be removed through sorption by in itu formed Fe_xO_x during the reaction. Kralchevska et al. (2016) tested the removal of phosphate by ferrate. It was confirmed that the phosphates were removed

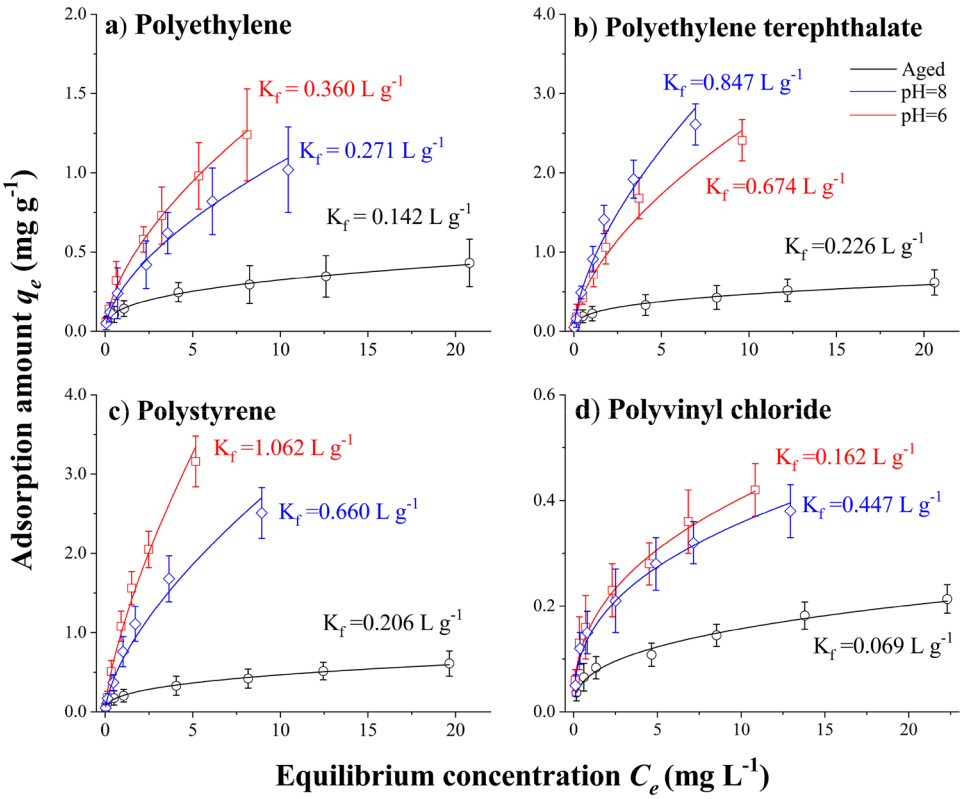

Fig. 5 Sorption of ciprofloxacin on microplastics. Experimental conditions: $[K_2FeO_4]_0$ = 10 mg L^{-1}, pH = 6 and 8, reaction time = 30 min, MP size = 6.5 μm

from water by the sorption of Fe_xO_x nanoparticles. Herein, the enhanced sorption capacities implied that MP-Fe_xO_x had high potential as contaminant-enriched vectors. Furthermore, the ferrate pre-oxidation could also improve the removal of organic contaminants and MPs in water synchronously.

Sinking behavior

Polymer types, associated with different densities, dominated the sinking ratio of aged MPs (Fig. 6, Table S4). Aged PE tended to float since PE has a density of 0.92 g cm^{-3} close to water. The other three MPs had densities higher than water. Their sinking ratios raised as the densities increased, e.g., nearly all aged PS (1.04 g cm^{-3}) maintained on the water surface, but > 50% of aged PVC (1.42 g cm^{-3}) tended to sink (Fig. 6c). Particle size also affected the sinking. Taking aged PET as an example, its sinking ratio declined as the size decreased. Approximate 55% 500 μm PET sank on the bottom, but nearly all 6.5 μm PET floated on the surface. Because the smaller the MPs, the greater the surface tension in the water, which hinders the sinking of MPs.

The sinking behavior of MPs can be explained as a seesaw of buoyance, gravity, and MP-water interface force (surface

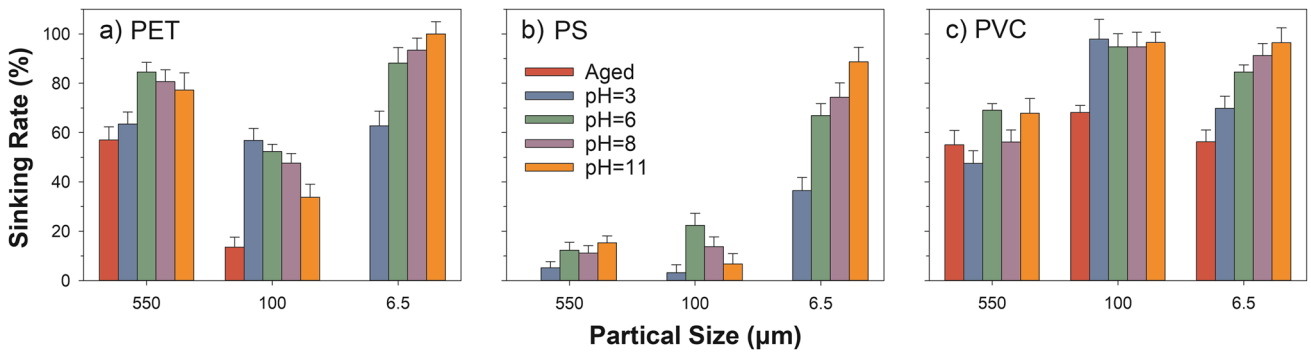

Fig. 6 Sinking ratio variations of microplastics. Experimental conditions: $[K_2FeO_4]_0$ = 10 mg L^{-1}, pH = 3, 6, 8, 11, reaction time = 30 min. Standard deviation was obtained from 3 independent samples

tension). When the buoyance dominates, MPs float, such as PE and PS. On the contrary, MPs with high density, such as PVC, are dominated by gravity and sink easily. Furthermore, if the magnitude of buoyance and gravity is close here (e.g., PET), the contribution of MP-water interface force becomes important. The decreasing size of PET increases their MP-water interface force, resulting in the declining sinking ratio (Fig. 6a).

The sinking behaviors of MPs were changed by ferrate oxidation. Generally, small MPs were more susceptible to ferrate oxidation. The sinking ratios of aged PS were zero. After pH 11 ferrate oxidation, it increased to 90% for 6.5 µm PS, much higher than 10% for 500 µm PS. This could be due to the generation of MP-Fe_xO_x complexes, which increased their densities (Tables S4–S6), resulting in a rising gravity and a higher sinking ratio. For example, the density of 6.5 µm PS increased 40% after ferrate oxidation at pH 11, while it maintained the same for 500 µm one. Similar phenomena were also observed for PET and PVC.

The effect of ferric oxide attachment on the density of large MPs (500 µm and 100 µm) was slight. Thus, variation of MP-water interface force induced by ferrate oxidation became a dominant factor. Ferrate presented a stronger oxidative capacity under acid conditions (Sharma et al. 2015), with a more significant hydrophobicity decrease (Table S7). As a result, the MP-water interface force decreased more dramatically, and a higher sinking ratio was observed (Fig. 6). The sinking ratio of 100 µm PET treated by pH 3 ferrate oxidation increased ~ 40% but weakened as pH increased (Fig. 6a). However, the sinking ratio of 6.5 µm MPs increased as pH raised, suggesting the dominating role of density variation. Higher pH can generate more Fe_xO_x attachment (Yang et al. 2018), contributing to a more significant increase in density (Table S6). The gradual improvement of sinking ratios as pH increased was observed for PET, PS, and PVC, which all verified this hypothesis (Fig. 6).

Moreover, surface oxidation on MPs can enhance the MP hydrophilicity (Table S7). The contact angle of MPs declined from ~ 90° to ~ 20° after acid ferrate oxidation, suggesting that the surface of MPs was transformed from relatively hydrophobic to hydrophilic. These variations decreased the MP-water interface force of MPs, contributing to the sinking of MPs.

The sinking performance variation generally resulted from interactions between buoyance/gravity (density) and MP-water interface force (size and hydrophobicity) (Fig. S5). The small MPs showed a greater improvement in sinking after ferrate pre-oxidation, which will facilitate MP sedimentation and removal during subsequent sedimentation processes. It might also be crucial for drinking water treatment since the most persistent MPs in DWTPs were identified as small ones (most < 10 µm). Of note, PE presented high tolerance against ferrate oxidation.

Conclusion

After ferrate oxidation, MPs were transformed into MP-Fe_xO_x complexes, mainly Fe_2O_3 and FeOOH. The attachment of Fe_xO_x enhanced the sorption capacities of organic matter on all MPs. Furthermore, it promoted the sinking of PET, PS, and PVC. Small MP sinking performance was enhanced, e.g., the sinking ratio of 6.5 µm PS increased by 70% after pH 6 oxidation. This suggested that some organic contaminants, such as CIP, in water can be enriched onto MP-Fe_xO_x complexes and can be easily removed together by sedimentation after ferrate oxidation. However, PE with different sizes was persistently floated, which should be paid specific attention to.

Supplementary Information The online version contains supplementary material available at https://doi.org/10.1007/s11356-023-26222-y.

Author contribution All authors contributed to the study conception and design. Material preparation, data collection, and analysis were performed by Yuheng Chen, Xinni Wu, and Jianwei Fu. The first draft of the manuscript was written by Ruijuan Liu and Huase Ou. All authors commented on previous versions of the manuscript. All authors read and approved the final manuscript.

Funding This project is supported by the National Natural Science Foundation of China (Grant No. 51778270) and Guangzhou Basic and Applied Basic Research Foundation (202102080273).

Data availability No. of figures: 6.

Declarations

Ethics approval and consent to participate Not applicable.

Consent for publication Not applicable.

Conflict of interest The authors declare no competing interests.

References

2011 Code for Design of Algae Water Treatment, Ministry of Housing and Urban-Rural Development of the People's Republic of China (MOHURD), Beijing

Anderson PJ, Warrack S, Langen V, Challis JK, Hanson ML, Rennie MD (2017) Microplastic contamination in Lake Winnipeg, Canada. Environ Pollut 225:223–231

Biesinger MC, Payne BP, Grosvenor AP, Lau LWM, Gerson AR, Smart RSC (2011) Resolving surface chemical states in XPS analysis of first row transition metals, oxides and hydroxides: Cr, Mn, Fe, Co and Ni. Appl Surf Sci 257:2717–2730

Chen Y, Liu R, Wu X, Liu Y, Fu J, Ou H (2022) Surface characteristic and sinking behavior modifications of microplastics during potassium permanganate pre-oxidation. J Hazard Mater 422:126855

Di M, Wang J (2018) Microplastics in surface waters and sediments of the Three Gorges Reservoir, China. Sci Total Environ 616:1620–1627

Fan J, Lin B-H, Chang C-W, Zhang Y, Lin T-F (2018) Evaluation of potassium ferrate as an alternative disinfectant on cyanobacteria

inactivation and associated toxin fate in various waters. Water Res 129:199–207
Guzzetti E, Sureda A, Tejada S, Faggio C (2018) Microplastic in marine organism: environmental and toxicological effects. Environ Toxicol Pharmacol 64:164–171
Hettithanthri O, Rajapaksha AU, Keerthanan S, Ramanayaka S, Vithanage M (2022) Colloidal biochar for enhanced adsorption of antibiotic ciprofloxacin in aqueous and synthetic hydrolyzed human urine matrices. Chemosphere 297:133984
Huang ZS, Wang L, Liu YL, Jiang J, Xue M, Xu CB, Zhen YF, Wang YC, Ma J (2018) Impact of phosphate on ferrate oxidation of organic compounds: an underestimated oxidant. Environ Sci Technol 52:13897–13907
Jiang Y, Goodwill JE, Tobiason JE, Reckhow DA (2016) Impacts of ferrate oxidation on natural organic matter and disinfection byproduct precursors. Water Res 96:114–125
Jin P, Song J, Wang XC, Jin X (2018) Two-dimensional correlation spectroscopic analysis on the interaction between humic acids and aluminum coagulant. J Environ Sci 64:181–189
Jun M, Wei L (2002) Effectiveness of ferrate (VI) preoxidation in enhancing the coagulation of surface waters. Water Res 36:4959–4962
Koelmans AA, Nor NHM, Hermsen E, Kooi M, Mintenig SM, De France J (2019) Microplastics in freshwaters and drinking water: critical review and assessment of data quality. Water Res 155:410–422
Kralchevska RP, Prucek R, Kolarik J, Tucek J, Machala L, Filip J, Sharma VK, Zboril R (2016) Remarkable efficiency of phosphate removal: Ferrate(VI)-induced in situ sorption on core-shell nanoparticles. Water Res 103:83–91
Lahens L, Strady E, Kieu-Le T-C, Dris R, Boukerma K, Rinnert E, Gasperi J, Tassin B (2018) Macroplastic and microplastic contamination assessment of a tropical river (Saigon River, Vietnam) transversed by a developing megacity. Environ Pollut 236:661–671
Lasch P, Noda I (2019) Two-dimensional correlation spectroscopy (2D-COS) for analysis of spatially resolved vibrational spectra. Appl Spectrosc 73:359–379
Law KL, Thompson RC (2014) Microplastics in the seas. Science 345:144–145
Liao N, Gu X, Wang Y, Xu H, Fan Z (2020) Analyzing macro-level ecological change and micro-level farmer behavior in Manas River Basin. China Land 9:250
Lima ARA, Costa MF, Barletta M (2014) Distribution patterns of microplastics within the plankton of a tropical estuary. Environ Res 132:146–155
Lin J, Yan D, Fu J, Chen Y, Ou H (2020) Ultraviolet-C and vacuum ultraviolet inducing surface degradation of microplastics. Water Res 186:116360
Lin J, Wu X, Liu Y, Fu J, Chen Y, Ou H (2022) Sinking behavior of polystyrene microplastics after disinfection. Chem Eng J 427:130908
Liu P, Qian L, Wang H, Zhan X, Lu K, Gu C, Gao S (2019) New insights into the aging behavior of microplastics accelerated by advanced oxidation processes. Environ Sci Technol 53:3579–3588
Lv D, Zheng L, Zhang H, Deng Y (2018) Coagulation of colloidal particles with ferrate(vi). Environ Sci: Water Res Technol 4:701–710
Ma J, Liu W (2002) Effectiveness and mechanism of potassium ferrate(VI) preoxidation for algae removal by coagulation. Water Res 36:871–878
Mao R, Lang M, Yu X, Wu R, Yang X, Guo X (2020) Aging mechanism of microplastics with UV irradiation and its effects on the adsorption of heavy metals. J Hazard Mater 393:122515
Mintenig SM, Loeder MGJ, Primpke S, Gerdts G (2019) Low numbers of microplastics detected in drinking water from ground water sources. Sci Total Environ 648:631–635
Moulder JF, Stickle WF, Sobol PE, Bomben KD (1992) Handbook of x-ray photoelectron spectroscopy. Perkin-Elmer Corporation 40:221
Novotna K, Cermakova L, Pivokonska L, Cajthaml T, Pivokonsky M (2019) Microplastics in drinking water treatment—current knowledge and research needs. Sci Total Environ 667:730–740
Prucek R, Tucek J, Kolarik J, Filip J, Marusak Z, Sharma VK, Zboril R (2013) Ferrate(VI)-induced arsenite and arsenate removal by in situ structural incorporation into magnetic iron(III) oxide nanoparticles. Environ Sci Technol 47:3283–3292
Sharma VK, Zboril R, Varma RS (2015) Ferrates: greener oxidants with multimodal action in water treatment technologies. Acc Chem Res 48:182–191
Su L, Xue Y, Li L, Yang D, Kolandhasamy P, Li D, Shi H (2016) Microplastics in Taihu Lake, China. Environ Pollut 216:711–719
Ta AT, Babel S (2020) Microplastic contamination on the lower Chao Phraya: abundance, characteristic and interaction with heavy metals. Chemosphere 257:127234
Uurasjarvi E, Hartikainen S, Setala O, Lehtiniemi M, Koistinen A (2020) Microplastic concentrations, size distribution, and polymer types in the surface waters of a northern European lake. Water Environ Res 92:149–156
Vethaak AD, Legler J (2021) Microplastics and human health. Science 371:672–674
Vianello A, Boldrin A, Guerriero P, Moschino V, Rella R, Sturaro A, Da Ros L (2013) Microplastic particles in sediments of Lagoon of Venice, Italy: first observations on occurrence, spatial patterns and identification. Estuar Coast Shelf Sci 130:54–61
Xie P, Chen Y, Ma J, Zhang X, Zou J, Wang Z (2016) A mini review of preoxidation to improve coagulation. Chemosphere 155:550–563
Yamashita T, Hayes P (2006) Effect of curve fitting parameters on quantitative analysis of $Fe_{0.94}O$ and Fe_2O_3 using XPS. J Electron Spectrosc Relat Phenom 152:6–11
Yamashita T, Hayes P (2008) Analysis of XPS spectra of Fe^{2+} and Fe^{3+} ions in oxide materials. Appl Surf Sci 254:2441–2449
Yang T, Wang L, Liu Y, Jiang J, Huang Z, Pang S-Y, Cheng H, Gao D, Ma J (2018) Removal of organoarsenic with ferrate and ferrate resultant nanoparticles: oxidation and adsorption. Environ Sci Technol 52:13325–13335
Zbyszewski M, Corcoran PL (2011) Distribution and degradation of fresh water plastic particles along the beaches of Lake Huron, Canada. Water Air Soil Pollut 220:365–372
Zhang K, Xiong X, Hu H, Wu C, Bi Y, Wu Y, Zhou B, Lam PKS, Liu J (2017) Occurrence and characteristics of microplastic pollution in Xiangxi Bay of Three Gorges Reservoir, China. Environ Sci Technol 51:3794–3801
Zheng L, Feng H, Liu Y, Gao J, Sarkar D, Deng Y (2021) Chemically enhanced primary treatment of municipal wastewater with ferrate(VI). Water Environ Res 93:817–825
Zhou Z, Jiang J-Q (2015) Reaction kinetics and oxidation products formation in the degradation of ciprofloxacin and ibuprofen by ferrate(VI). Chemosphere 119:S95–S100
Zhou S, Shao Y, Gao N, Zhu S, Li L, Deng J, Zhu M (2014) Removal of Microcystis aeruginosa by potassium ferrate (VI): impacts on cells integrity, intracellular organic matter release and disinfection by-products formation. Chem Eng J 251:304–309